Monte Carlo simulation for bremsstrahlung and photoneutron yields in high-energy x-ray radiography*

Xu Hai-Bo(许海波)†, Peng Xian-Ke(彭现科), and Chen Chao-Bin(陈朝斌)

Institute of Applied Physics and Computational Mathematics, Beijing 100094, *China*

(Received 17 August 2009; revised manuscript received 12 November 2009)

This paper reports on the results of calculations using a Monte Carlo code (MCNP5) to study the properties of photons, electrons and photoneutrons obtained in the converted target and their transportations in x-ray radiography. A comparison between measurements and calculations for bremsstrahlung and photoneutrons is presented. The radiographic rule and the effect of the collimator on the image are studied with the experimental model. The results provide exact parameters for the optimal design of radiographic layout and shielding systems.

Keywords: x-ray radiography, bremsstrahlung, photoneutron, energy spectrum, angular distribution
PACC: 2915D, 8170J

1. Introduction

Explosively driven hydrodynamic tests utilize very powerful x-ray sources to radiograph a full-scale, non-nuclear mock-up of a nuclear weapon primary during the late stages of the implosion, returning data on shapes, densities, and edge locations. In dynamic x-ray radiography, a pulsed, high-energy accelerator produces an intense beam of electrons that is focused onto a bremsstrahlung converter target. Interactions between the electrons and the converter target generate an x-ray pulse to image the internal structure of a dynamically evolving object. Accurate electron and photon transport models are needed to describe the radiation source and to analyse the resulting radiograph. As the photons traverse an object, they may be absorbed or scattered by the intervening material. Absorption leads to the attenuation of the incident photon intensity and the scatter results in a nonuniform radiation background.[1] In addition to the experimental object, shielding material, collimators and other apparatus can attenuate or scatter photons within the radiographic system. Finally, the detector adds a nonuniform background distribution. Each of these contributions must be taken into account to fully analyse data from the object.

Such photon, electron and neutron spectra are difficult to measure with the standard nuclear instrumentation, due to the high flux and the pulsed radiation field. Therefore a computer code allowing a suitable simulation of the entire process of photon, electron and neutron generation and transport from the converted target to the film is required. Version MCNP5 is used in the simulations, which is a recent Monte Carlo code for solving radiation transport problems related to neutrons, photons, electrons and coupled neutron–photons or electron–photons in various media.[2,3] The photonuclear capabilities have been included in MCNP5 by introducing the LA150U photonuclear library, which contains photonuclear cross sections for 12 isotopes only. In this paper, we have taken all the required photonuclear reaction cross sections from recent tabulations.

An outline of the rest of the paper is as follows. A comparison between measurements and the MCNP5 code calculations is given in Section 2. The calculations of bremsstrahlung production and associated leakage electron and photoneutron production in the tantalum target irradiated by electron beams with energy 20 MeV are given in Section 3. In Section 4, we obtain the photon and the photoneutron distributions at the film plane. Finally, the main results are discussed and summarized in Section 5.

*Project supported by the National Natural Science Foundation of China (Grant No. 10576006) and the Foundation of China Academy of Engineering Physics (Grant Nos. 2007A01001 and 2009B0202020).

†Corresponding author. E-mail: hbxu2002@yahoo.com.cn

© 2010 Chinese Physical Society and IOP Publishing Ltd

2. Measurements and MCNP5 code calculations

In the first step, the proper functioning of the code is checked by comparing simulation results with measurement results. The calculated results and the experimental results are shown in Figs. 1 and 2. The calculated results and the experimental results are found to be in good agreement.

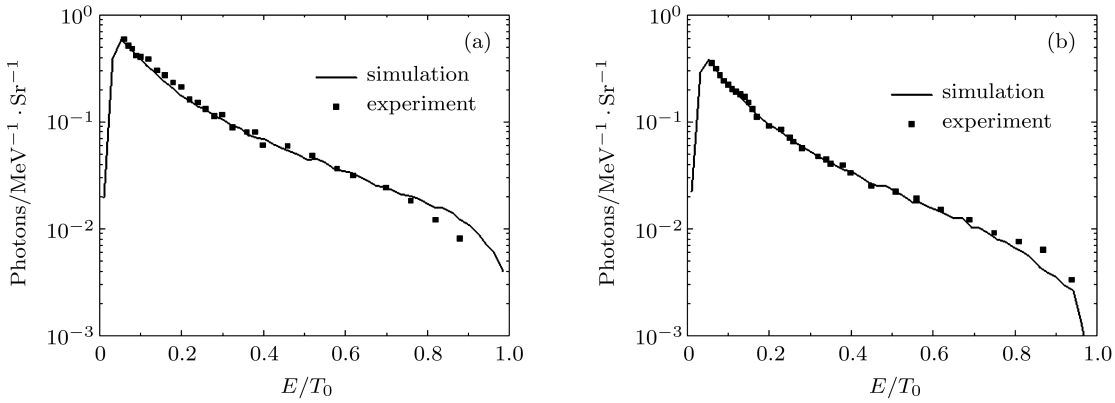


Fig. 1. Comparisons between calculated and experimental bremsstrahlung spectra at emergence angles (a) 0° and (b) 12°.

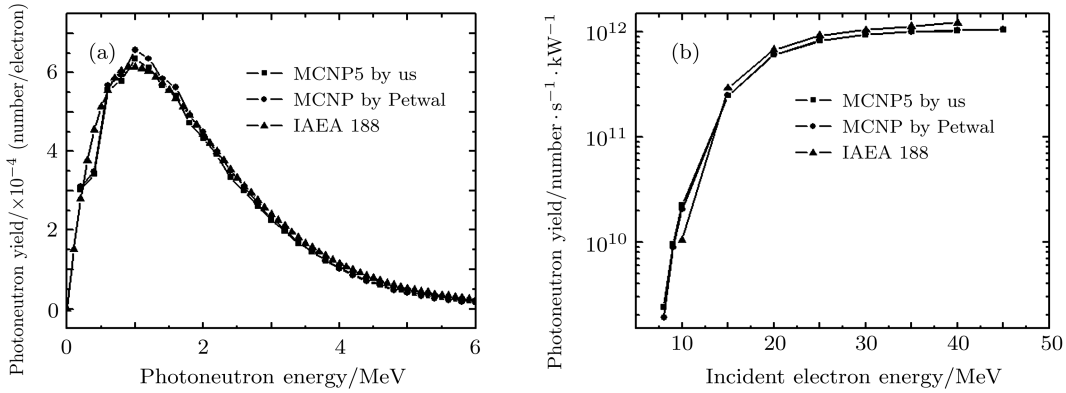


Fig. 2. Comparisons of photoneutron spectrum and yield: (a) photoneutron spectrum with the electron kinetic energy 45 MeV; (b) photoneutron yield with different incident electron energies.

When high-energy electrons impinge on a target material, a continuous spectrum of bremsstrahlung photons is generated. These bremsstrahlung photons subsequently interact with the nucleus of the target material, resulting in the emission of nucleons. This interaction is known as a photonuclear interaction. Figure 1 shows a comparison between the spectrum of bremsstrahlung photons per incident electron emitted from a 5.80-g/cm^2 thick tungsten target, at emergence angles 0° and 12° . In the calculations, the monoenergetic, zero-width beam of electrons is incident perpendicularly on the target with the kinetic energy $T_0 = 9.66$ MeV. For comparison, the bremsstrahlung spectra for directions of emergence at 0° and 12° produced by 9.66-MeV electrons in tungsten were measured by Starfelt and Koch with NaI scintillation counters.[4,5] In the experiment, the energy dispersion of incident electrons was approximately to 4%.

As the nucleons are bounded with the nucleus by the binding energy (5–15 MeV), the photon should have an energy above a threshold value to participate in the photonuclear reaction. Absorption of the incident photons leads the nucleus to be excited into a higher discrete energy state, and the extra energy is emitted in the form of neutrons. For heavy nuclei, the excited nucleus comes into the ground state by the emission of a neutron (γ, n). Some contribution from double neutron emission (γ, xn) is also possible

for higher photon energies. Because of the presence of the large Coulomb barrier, proton emission is strongly suppressed for heavy nuclei. The cross section for this process has a maximum at a photon energy between 13–18 MeV for heavy nuclei and 20–23 MeV for light nuclei ($A < 40$). Though neutron yield depends sensitively on the material species and the geometry of the target, for comparing the results and ascertaining the proper functioning of photonuclear physics included in the code, we have considered a lead target, for which measured results are published in IAEA 188.[6,7] In the experiment, the lead target is of a cylindrical pallet with $r = 3$ cm and thickness 1.68 cm. Figure 2 shows a comparison of the photoneutron spectrum and the photoneutron yield from the lead target. The incident electrons are monoenergetic and incident perpendicularly on the target.

3. Photons, electrons and photoneutrons from the tantalum target

In this section are described the calculations of bremsstrahlung production and associated leakage electron production, photoneutron production from the tantalum target irradiated by an electron beam with kinetic energy 20 MeV.

We assume that the electron beam satisfies the Gauss distribution and has an axial symmetry in phase space,

$$f(r,\theta) = \frac{1}{2\pi\sigma_r\sigma_\theta}\exp\left[-\frac{1}{2}\left(\frac{r^2}{\sigma_r^2}+\frac{\theta^2}{\sigma_\theta^2}\right)\right]. \quad (1)$$

The normalized emittance and the full width at half-maximum (FWHM) can be defined as

$$\varepsilon = \gamma\beta\varepsilon_{\rm rms} = 4\gamma\beta\sigma_r\sigma_\theta, \quad (2)$$

$$\text{FWHM} = 2\sqrt{2\ln 2}\sigma_r, \quad (3)$$

where γ is the relativistic mass and β is the relativistic velocity. In our study, we have used a 20-MeV electron linear accelerator, which has a normalized emittance of 400 cm-mrad and an FWHM of 3 mm.[8]

The bremsstrahlung intensity depends sensitively on the target thickness and emergence angle. The region of interest is the field of view within the conical hole of the collimator. In high-energy x-ray radiography, the taper angle is about 2°. Figure 3(a) shows the bremsstrahlung intensity as a function of target thickness. We can see that the maximum intensity within the angle of 2° occurs between thicknesses of 1.0 and 1.5 mm. Figure 3(b) shows the angular distributions with different thicknesses within the angle of 2°. We can see that the bremsstrahlung field uniformity with a 1.5-mm thick target is better than that with a 1.0-mm thick target. Therefore, we choose a 1.5-mm thick target in the following calculations.

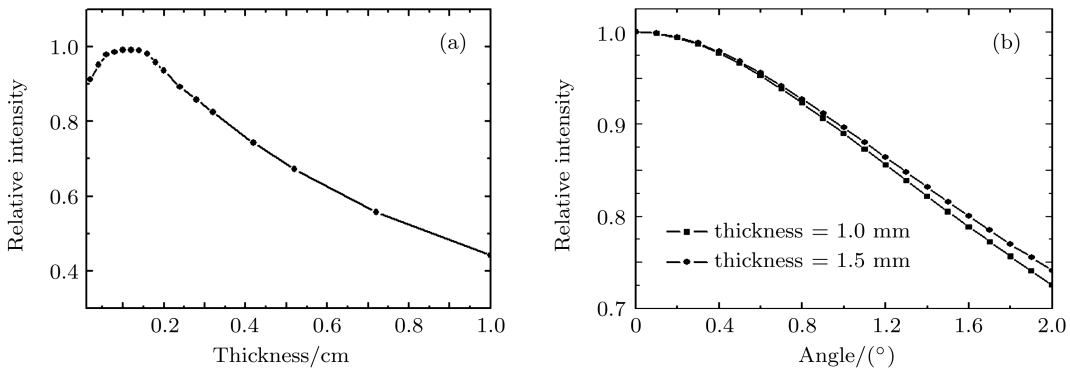


Fig. 3. (a) Bremsstrahlung intensity as a function of the target thickness; (b) angular distribution with different target thicknesses within angle 2°.

The bremsstrahlung efficiency η can be defined as the fraction of the kinetic energy T_0 of the incident electrons which emerges in the form of bremsstrahlung from the target. Taken into account in the efficiency is the reduction of bremsstrahlung production due to the leakage of electrons from the target and the attenuation of bremsstrahlung within the target.[4] The photon, the electron and the photoneutron yields from tantalum are given in Table 1. The efficiency in the x-ray radiography is $\eta = 5.044/20 = 25.22\%$.

Table 1. Photon, electron and photoneutron yields from tantalum per incident electron.

yields	photon		electron		photoneutron	
	total	2°	total	2°	total	2°
number	2.17	2.70×10^{-2}	0.95	2.48×10^{-3}	2.00×10^{-4}	6.44×10^{-8}
energy/MeV	5.04	8.96×10^{-2}	10.82	3.30×10^{-2}	2.09×10^{-4}	6.05×10^{-8}
average energy/MeV	2.32	3.32	11.39	13.31	1.05	1.06

3.1. Angular distribution of photons, electrons and photoneutrons

The emergent bremsstrahlung is always accompanied by some transmitted electrons and photoneutrons. The calculations of bremsstrahlung photons, photoneutrons and leakage electrons from the Ta target per incident electron as a function of emergence angle are shown in Figs. 4(a), 4(b) and 4(c) respectively.

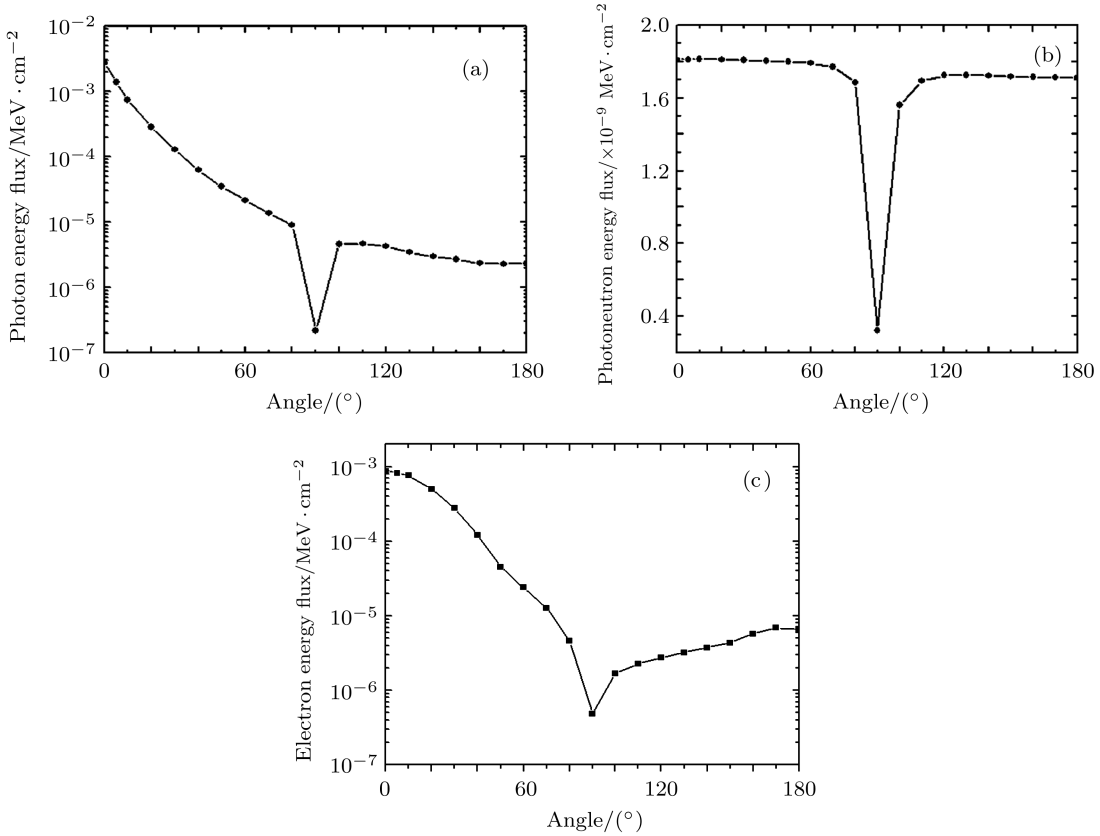


Fig. 4. Energy fluxes from tantalum target per incident electron as a function of emergence angle for (a) photons, (b) photoneutrons, and (c) electrons.

The curves for angular dependencies of photon energy flux and electron energy flux each have a rather sharp peak in the forward direction, then a rapid decrease at larger angles and a very pronounced dip around 90°, followed by a flattening distribution at backward angles beyond 90°. The intensity pertains to the emergent photon current and vanishes at 90° for the assumed plane-parallel target that is finite in the z direction but infinite in the x and y directions.[9] For a more realistic target of finite lateral dimensions, this assumption may be not true and the dip of intensity around 90° may be much less pronounced.

In the photon energy range of 10–30 MeV, photoneutron production results from the giant photonuclear resonance mechanism. Neutron angular distribution is usually assumed to be isotropic, since direct

neutrons, characterized by a $\sin^2\theta$ angular distribution (θ is the angle between the photon and neutron direction), represent only a small percentage of the entire spectrum, while neutrons generated by the evaporative process are isotropically emitted.

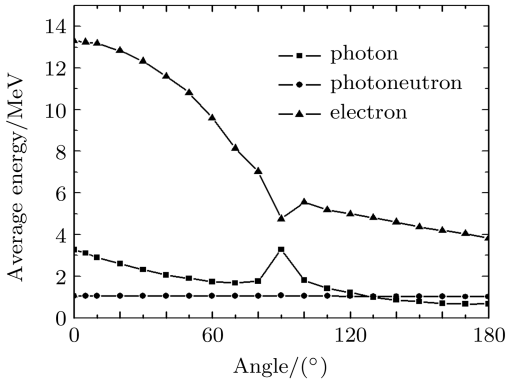


Fig. 5. Average energies from the tantalum target as a function of emergence angle.

Figure 5 shows the average energies of bremsstrahlung photons, leakage electrons and photoneutrons from the Ta target as a function of emergence angle. We can see that the leakage electrons still have very high energies. For thin targets these are mainly primary electrons.

3.2. Energy spectra of photons, electrons and photoneutrons

The calculated spectra of bremsstrahlung photons, photoneutrons and leakage electrons from the Ta target per incident electron for the two angles of 0° and 20° are shown in Figs. 6(a), 6(b) and 6(c). It can be seen that the closer to 0° the emergence angle is, the harder the spectrum peak will be. This is because energetic photons can be emitted only by electrons that have lost little energy and have not yet been deflected much by multiple scattering.

The spectrum of the photoneutron can be well described by a Maxwellian distribution, which is dominated by low energy neutrons peaking at about 0.50 MeV.

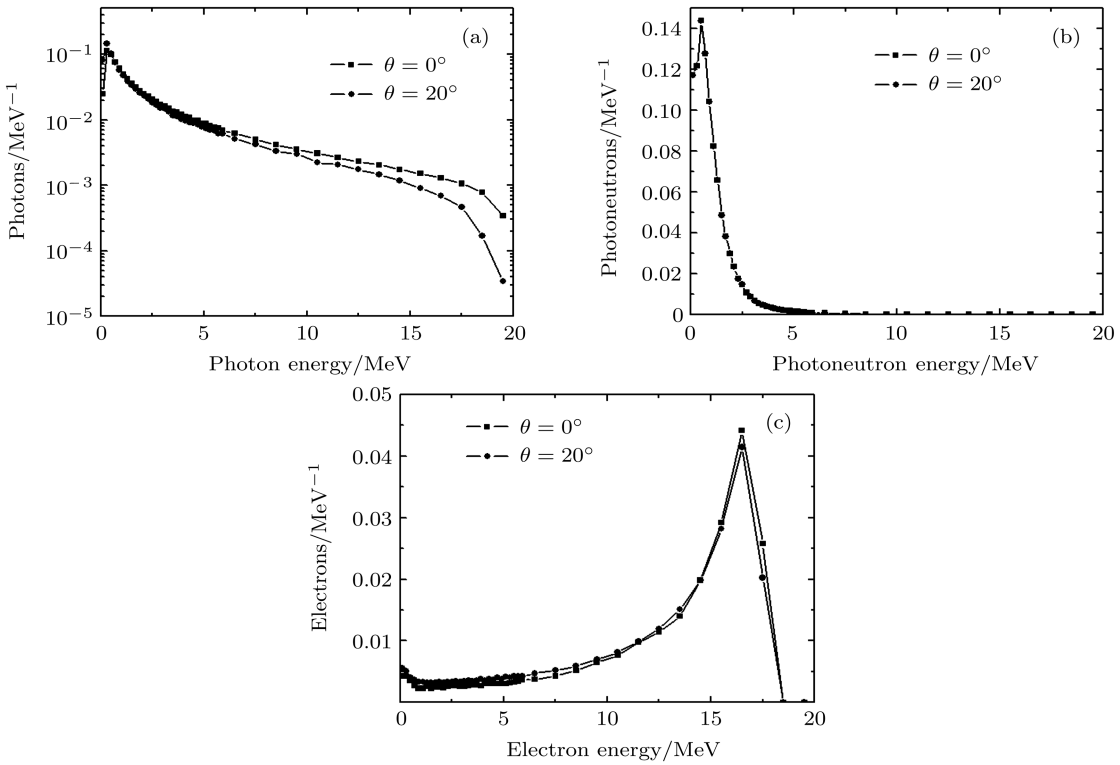


Fig. 6. Spectra from the tantalum target per incident electron for (a) photons, (b) photoneutrons, and (c) electrons.

The fitted equation of the distribution is

$$\frac{\mathrm{d}N}{\mathrm{d}E} = k\frac{E}{T^2}\,\mathrm{e}^{-E/T}, \tag{4}$$

where T is the nuclear temperature (MeV), which is characteristic of a particular target nucleus and represents the most probable energy of the neutrons generated. Nuclear temperature T is found to be 0.5 MeV for Ta.

4. Radiography

The Monte Carlo code models electron transport and photon generation in the target and interrogation of the object by the photons. We use this capability to generate synthetic radiographs of the French test object (FTO), which was designed to allow French and U.S. experimenters to collaborate on high-energy x-ray radiography methods and analysis, and their detection.

The Monte Carlo code is used to simulate the propagation of photons through the FTO. In these calculations, the FTO is placed 2 m away from the source and the detector is 1 m away behind the object. Table 2 shows the materials and structures of the FTO model.

Table 2. French test object model.

material	void	uranium (238)	copper
outer radius/cm	1.0	4.5	6.5
density/g·cm^{-3}	0.0	18.9	8.9

The imaging objectives were confined to the metallic components of the test object, so the first step in collimating the source was to build a lead wall 0.6 m high, 0.6 m wide and 0.2 m thick with a conical hole in the centre. The taper of the cone originates at the source. A simplified radiographic process is schematically shown in Fig. 7 with $\phi_1 = 3.2$ cm, $\phi_2 = 4.0$ cm for the main collimator and $\phi_1 = 7.54$ cm, $\phi_2 = 3.0$ cm for the graded collimator. Dimensions were chosen such that the field of view in the object plane was larger in diameter than the copper sphere.

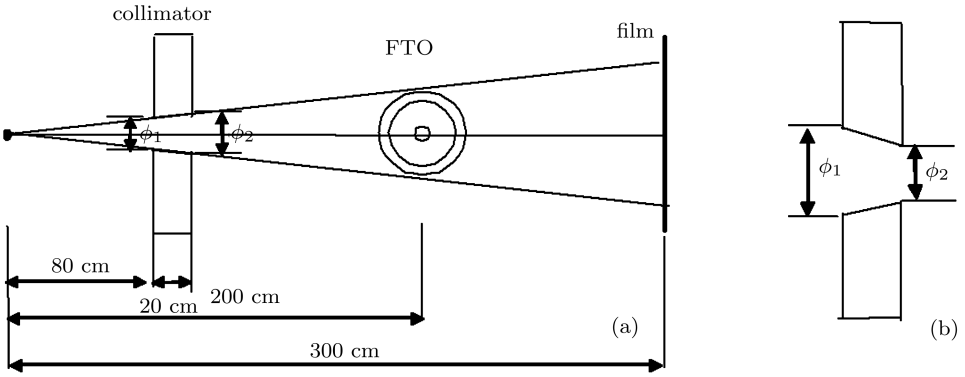


Fig. 7. (a) A sketch of the simplified radiographic process, and (b) the geometry of the graded collimator.

To avoid reducing transmission associated with the main collimator, we employed a conical collimator whose taper originated near the object.[10,11] The goal is twofold: (i) to reduce the dynamic range of the information presented to the detector, (ii) to reduce the magnitude of the scattered radiation reaching the detector and characterize the spatial distribution of the residual scattered radiation field while still preserving a complete view of the object. In this situation the dynamic range was reduced to manageable proportions, and we can see that the outer boundary of the copper as well as the void in the centre are both on one film. The scattered radiation does not appear to be a major problem.

The radius of the opening and the taper angle can be adjusted to cover many situations. Figure 8(a) shows one-dimensional radiographs of the photon energy flux as a function of radius at the film. Figure 8(b) exhibits their corresponding average energies. A densitometer scan of the image obtained with the graded collimator shows a reduced dynamic range, a rather clean central image, and sharp peaks at the uranium and copper outer boundaries.

Figure 9(a) shows the photoneutron energy flux as a function of radius at the film, and figure 9(b) exhibits their corresponding average energies. The mean energy of the neutron spectrum from the tantalum target,

generated by the (γ, n) reaction, is around 1 MeV, but in the film plane, neutrons have a more complicated distribution due to the transmission through the object and the collimator and a lower mean energy. The flux of photons at the film is much larger than that of neutrons. The graded collimator can minimize neutrons while the scatter photons are reduced.

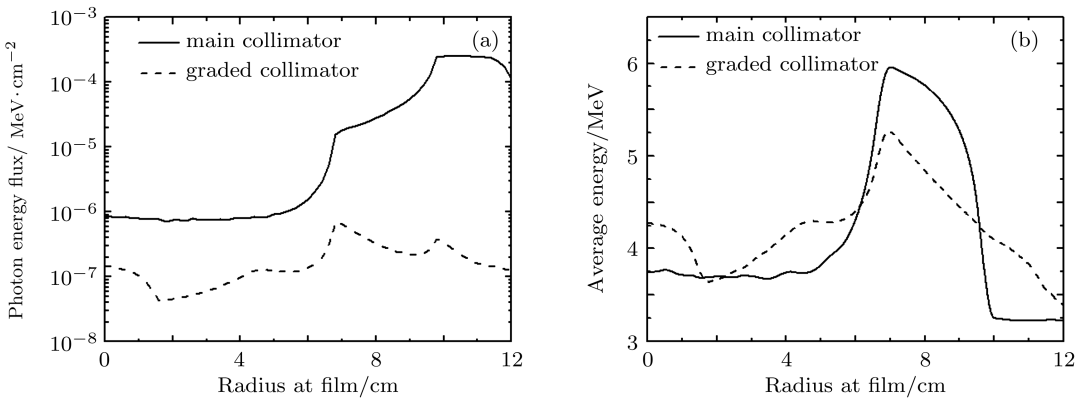


Fig. 8. Photon energy fluxes (a) and average energies (b) versus radius at the film.

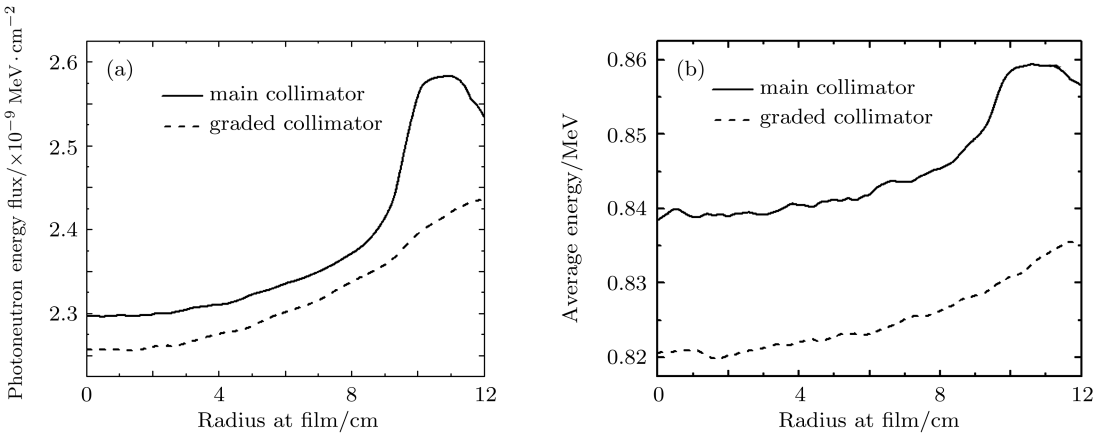


Fig. 9. Photoneutron energy fluxes (a) and average energies (b) versus radius at the film.

The energy flux of electrons through the dense object is very small because the penetrating ability of electrons is much less than that of photons and neutrons. In x-ray radiography, the electron at the film should be neglected.

5. Conclusions

In this paper are presented the calculation results obtained by using the Monte Carlo code (MCNP5) to study the properties of photons, electrons and photoneutrons obtained in the converted target and the static radiography of the FTO. Combining theoretical analyses with simulations, the following conclusions can be drawn: 1) the bremsstrahlung and the leakage electrons depend greatly on emergence angle, but the photoneutron angular distribution is roughly isotropic; 2) the yield of photoneutrons is much less than that of photons and electrons from the target; 3) the flux of photons at the film is much larger than that of neutrons; 4) the graded collimator can minimize neutrons while the scatter photons are reduced.

These data allow one to estimate the electron and neutron backgrounds at the film. The results provide a more detailed understanding of latent image formation and information for the optimal design of radiographic

layout and shielding systems.

References

[1] Kwan T J T, Mathews A R, Christenson P J and Snell C M 2001 *Comput. Phys. Commun.* **142** 263

[2] Brown F B, Barrett R F, Booth T E, Bull J S, Cox L J, Forster R A, Goorley T J, Mosteller R D, Post S E, Prael R E, Selcow E C, Sood A and Sweezy J 2002 *LA-UR02-3935*

[3] Xu M H, Liang T J and Zhang J 2006 *Acta Phys. Sin.* **55** 2357 (in Chinese)

[4] Martin J B and Stephen M S 1970 *Phys. Rev.* C **2** 621

[5] Starfelt N and Koch H W 1956 *Phys. Rev.* **102** 1598

[6] Seltzer S M and Berger M J 1973 *Phys. Rev.* C **7** 858

[7] Petwal V C, Senecha V K, Subbaiah K V, Soni H C and Kotaiah S 2007 *Pramana J. Phys.* **68** 235

[8] Shi J J, Liu J, Liu J and Li B Y 2007 *Chin. Phys.* **16** 266

[9] Wei X Y, Li Q F and Yan H Y 2009 *Acta Phys. Sin.* **58** 2313 (in Chinese)

[10] Mueller K H 1984 *Proc. 16*$^{\text{th}}$ *International Congress on High Photography and Photonics, Strasbourg* (SPIE, Bellingham, Wash., 1984) **491** 130

[11] Fahimi H and Macovski A 1989 *IEEE Trans. Med. Imaging* **8** 56